Journal of Thermal Analysis and Calorimetry (2018) 132:1277–1289
https://doi.org/10.1007/s10973-018-7015-3

Thermodynamic analysis of reduction in copper slag by biomass molding compound based on phase equilibrium calculating model

Zongliang Zuo[1] · Qingbo Yu[1] · Huaqing Xie[1] · Fan Yang[1] · Qin Qin[1]

Received: 12 October 2017 / Accepted: 16 January 2018 / Published online: 25 January 2018

Abstract
Copper slag is a good valuable material resource with high iron content in the form of fayalite. Biomass as reduction reducer was proposed in this paper. For the basic research of the reduction in biomass, the biomass reducer was simplified as molding compound C, CO, H_2 and CH_4. The reactions of $2FeO{\cdot}SiO_2$ with C, CO, H_2 and CH_4 could proceed spontaneously with the addition of CaO. The Gibbs free energy is decreased significantly by addition of CaO. The equilibrium compositions of products were calculated and analyzed combing with 19 basic reactions. Beginning temperature of C, CO, H_2 and CH_4 is 900, 623, 567 and 511 K, respectively The reduction degree of C, CH_4, H_2 and CO is 1, 0.851, 0.695 and 0.452, respectively, at 1773 K when the reducer addition ratio is 1.0 calculated by phase equilibrium calculating model. Direct reduction reaction of copper slag dominates at higher temperature, and temperature region of 700–1173 K is the transformational zone. Indirect reduction index curves are in the shape of reverse 'S,' and the higher temperature is in favor of indirect reduction in copper slag. There is a steady increase in reduction degree with the increase in reducer. Reduction reaction path of copper slag by C, CO, H_2 and CH_4 is established.

Keywords Phase equilibrium · Thermodynamic analysis · Reduction · Copper slag · Biomass molding compound

Introduction

Copper slag, an important potential iron ore secondary resource, can be widely found in copper smelting enterprise. For every ton of copper production, about 2.2 tons of copper slag is generated. [1]. The temperature of molten copper slag is above 1573 K, and the contents of iron in copper slag are 30–45%, whose grade is higher than that in some low-grade industrial iron ore [2, 3].

At present, copper slag is used in sand-blasting industry or used as certain value-added products, such as cement, concrete, fill, abrasive tools, abrasive materials, mineral wool and glass ceramics [1, 4–8]. The abundant iron in copper slag is wasted. For the shortage of high-grade iron ore resources in recent years, the utilization of copper slag for the extraction of iron attracted more attentions. Many practices have proved several methods recovering iron from copper slag. These methods include reduction method [9–14], oxidation method [15, 16], grinding flotation method [17] and magnetic separation method [18]. Among these methods, reduction method recovers iron by adding different kinds of carbonaceous materials and obtains higher Fe recovery ratio.

The type of reducers for the reduction in copper slag falls into two major categories, solid carbonaceous materials (coal, coke, graphite and anthracite) [11–13, 19] and gas reducers (H_2, CO, CH_4 and natural gas) [10, 20, 21]. Large amount of carbonaceous materials are consumed. In order to decrease the consumption of conventional reducers and meet the growing greenhouse challenges, incorporation of renewable energy sources to the existing and emerging metallurgical operations is desirable. Studies have been conducted to introduce biomass into metallurgical industries [22–26]. With biomass added, the iron ore was reduced to predominantly metallic iron. Biomass is a widely distributed, abundant, renewable and environment-friendly reducing agent [27]. It can replace fossil fuels to realize the reduction in copper slag. Due to the complexity

✉ Qingbo Yu
yuqb@smm.neu.edu.cn

[1] School of Metallurgy, Northeastern University, P.O. Box 345, No 11, Lane 3, Wenhua Road, Heping District, Shenyang, Liaoning, People's Republic of China

of kinds of biomass pyrolysis products, it is unrealistic to make clear every reaction of pyrolysis products and the reduction reactions of them. All in all, the fundamental reduction reactions in copper slag are iron oxide with C, CO, H_2 and CH_4. Therefore, the reduction reactions by C, CO, H_2 and CH_4 are the basic reactions of the reduction in iron oxide by biomass.

Thermodynamic studies on the standard Gibbs free energy changes (ΔG^{θ}) have been applied for feasibility analysis before practical experiments [28–32]. Some key reactions about reduction in copper slag are carried out by this method [33, 34]. Owing to the complex compositions of copper slag, the reactions involved in the reduction process are complicated. Therefore, the thermodynamic results obtained by ΔG^{θ} may not be representative of the real process. Besides, the formation of iron containing phase is difficult to investigate by key reactions. To establish internal reduction reaction mechanism and make clear the transformation behavior of the species in copper slag system, the main components of copper slag are taken into account. Based on Gibbs free energy principle and phase equilibrium calculating model in HSC Chemistry software, the detailed thermodynamic study was performed. The biomass reducer is simplified as molding compound C, CO, H_2 and CH_4, which are pyrolysis productions of biomass. The effects of reducer type, temperature and reducer addition ratio on products components, reduction degree and enthalpy are investigated.

Materials and methods

In this paper, copper slag was supplied from a flash smelting furnace in a copper smelting corporation. The chemical composition of copper slag in this paper is shown in Table 1. The phases of raw materials were identified by X-ray diffractometer (XRD). Figure 1 presents XRD patterns of the waste slag before the reduction reaction. Figure 1 indicates that fayalite and magnetite are the main mineral phases in slag. The contents in copper slag reduction system are simplified as Fe, Fe_3O_4, $2FeO{\cdot}SiO_2$, CaO, $CaCO_3$, MgO, SiO_2, Al_2O_3, Cu_2S, Zn, $2CaO{\cdot}SiO_2$, $3CaO{\cdot}SiO_2$, CO, CO_2, H_2, CH_4, H_2O, 18 kinds of chemical compositions. The equilibrium compositions were calculated by *phase equilibrium calculating model* of HSC Chemistry based on the minimization of the total Gibbs free energy. And the amount of the main contents was calculated by molar weight. The initial copper slag amount

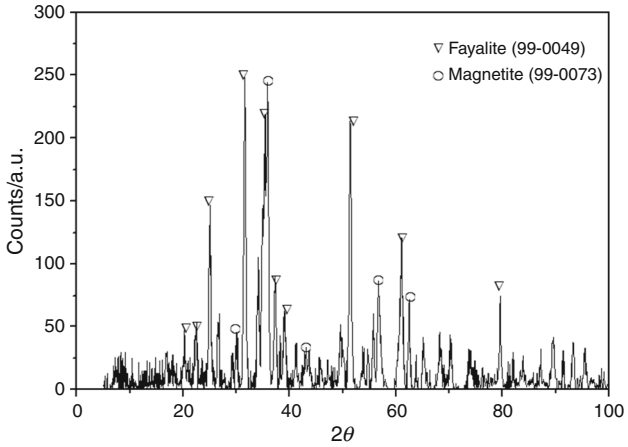

Fig. 1 X-ray diffraction spectrogram of copper slag

data and addition of reducer are shown in Tables 2, 3. The reducer addition ratio of C/O, CO/O and H_2/O is 1:1, and the reducer addition ratio of CH_4/O is 1:3. The CaO/SiO_2 ratio is 1:1. The theoretical molar quantity of 'O' in FeO and Fe_3O_4 is 0.848 kmol. And the addition reducer molar quantity of C, CO and H_2 is 0.848 kmol, and Fe production from copper slag is 0.788 kmol. The thermodynamic analysis is conducted taking the following assumed conditions into account:

1. The mass of copper slag is 100 kg, and the atmosphere pressure is 0.1 MPa.
2. Phases with contents lower than 0.5% in this paper are not discussed.
3. The biomass reducer is simplified as molding compound C, CO, H_2 and CH_4, which are the main pyrolysis productions of biomass. In order to make sure the reactivity characteristic of every reducer molding compound, C, CO, H_2 and CH_4 are not mixed together in reduction process.

According to the compositions of different kinds of reducer, the reduction reactions and equilibrium compositions are discussed (Table 3).

Results and discussion

Reactions of copper slag reduction system

Reactions of copper slag reaction system include direct reduction reactions of C [Eqs. (1)–(3)], indirect reduction reactions of CO [Eqs. (4)–(6)], reduction reactions of H_2

Table 1 The compositions of copper slag, mass %

FeO	Fe_3O_4	CaO	Al_2O_3	MFe	SiO_2	Cu	MgO	S	Zn	others
37.50	18.90	0.23	0.98	1.24	31.99	0.74	0.42	0.39	2.78	4.87

Table 2 Phase compositions of initial copper slag, kmol

$2FeO{\cdot}SiO_2$	Fe_3O_4	CaO	Al_2O_3	MFe	Cu_2S	MgO	Zn
0.260	0.082	0.004	0.010	0.022	0.012	0.011	0.043

Table 3 Molar quantity of reducer addition, kmol

C/kmol	CO/kmol	H_2/kmol	CH_4/kmol	'O'/kmol
C/O 1:1	CO/O 1:1	H_2/O 1:1	CH_4/O 1:3	
0.848	0.848	0.848	0.283	0.848

[Eqs. (7)–(9)] and CH_4 [Eqs. (10)–(12)], gasification reactions [Eqs. (13)–(14)], slagging reactions with CaO [Eqs. (15)–(18)] $CaCO_3$ conversion reaction [Eq. (19)] and cracking reaction of CH_4 [Eq. (20)].

Based on Gibbs principle of the minimization of the total Gibbs free energy, the reaction can proceed spontaneously when the Gibbs free energy change is lower than zero. Figure 2 shows the Gibbs free energy change curves of reactions with the change of temperature. For most reactions, Gibbs free energy decreases to lower than zero with the increase in temperature. However, the reduction in $2FeO{\cdot}SiO_2$ and FeO by CO and H_2 could not proceed spontaneously. Besides, the decompose reaction temperature of $CaCO_3$ is 1073 K, lower than the reduction temperature. $CaCO_3$ could not be generated in this reaction system in other words. For smelting reduction in iron ore, the reaction temperature should be above the melting point of sample. The melting point of copper slag is about 1473 K. Smelting reduction in copper slag is in the region of 1473–1673 K. Direct reduction in copper slag is lower than its melting point and at the region of 1173–1473 K, considering the initial reduction reaction temperature of copper slag. The value of Gibbs free energy change efficiently decreased with the addition of CaO as shown in Fig. 3. The reduction reactions are promoted in various degrees. The reactions of $2FeO{\cdot}SiO_2$ with CO and H_2 could proceed spontaneously above melting reduction temperature and direct reduction temperature with the addition of CaO. At 1373 K, the Gibbs free energy change decreases from 41–1242 kJ with the addition of CaO.

$$Fe_3O_4 + C = 3FeO + CO\ (g) \quad (1)$$

$$FeO + C = Fe + CO\ (g) \quad (2)$$

$$2FeO \cdot SiO_2 + 2C = 2Fe + 2CO\ (g) + SiO_2 \quad (3)$$

$$Fe_3O_4 + CO\ (g) = 3FeO + CO_2(g) \quad (4)$$

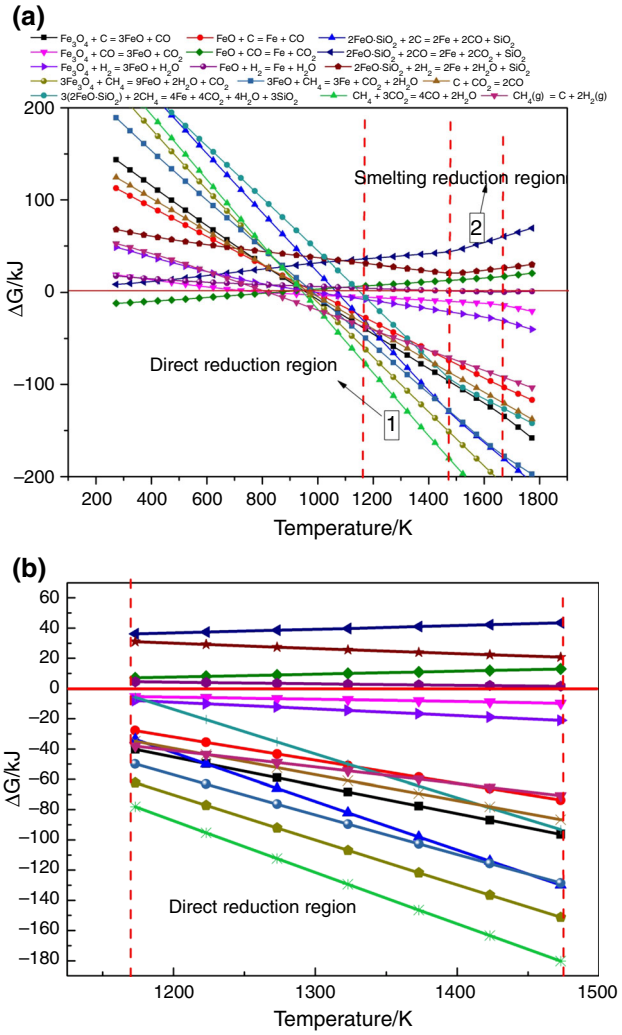

Fig. 2 Gibbs free energy change curves of reactions with change of temperature: **a** reactions 273–1773 K; **b** 1173–1473 K (direct reduction region)

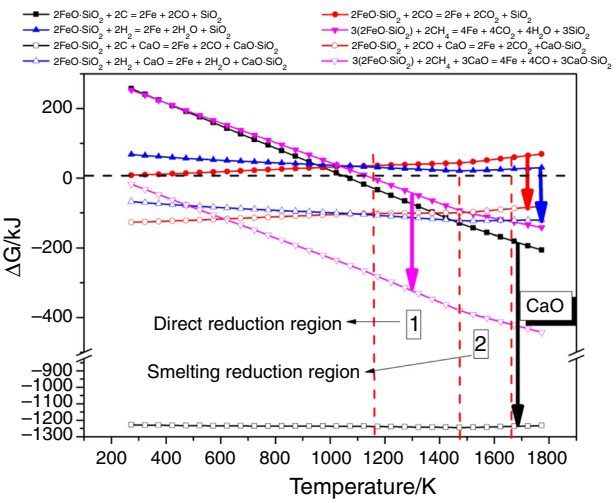

Fig. 3 Effects of CaO on the reactions of Gibbs free energy change

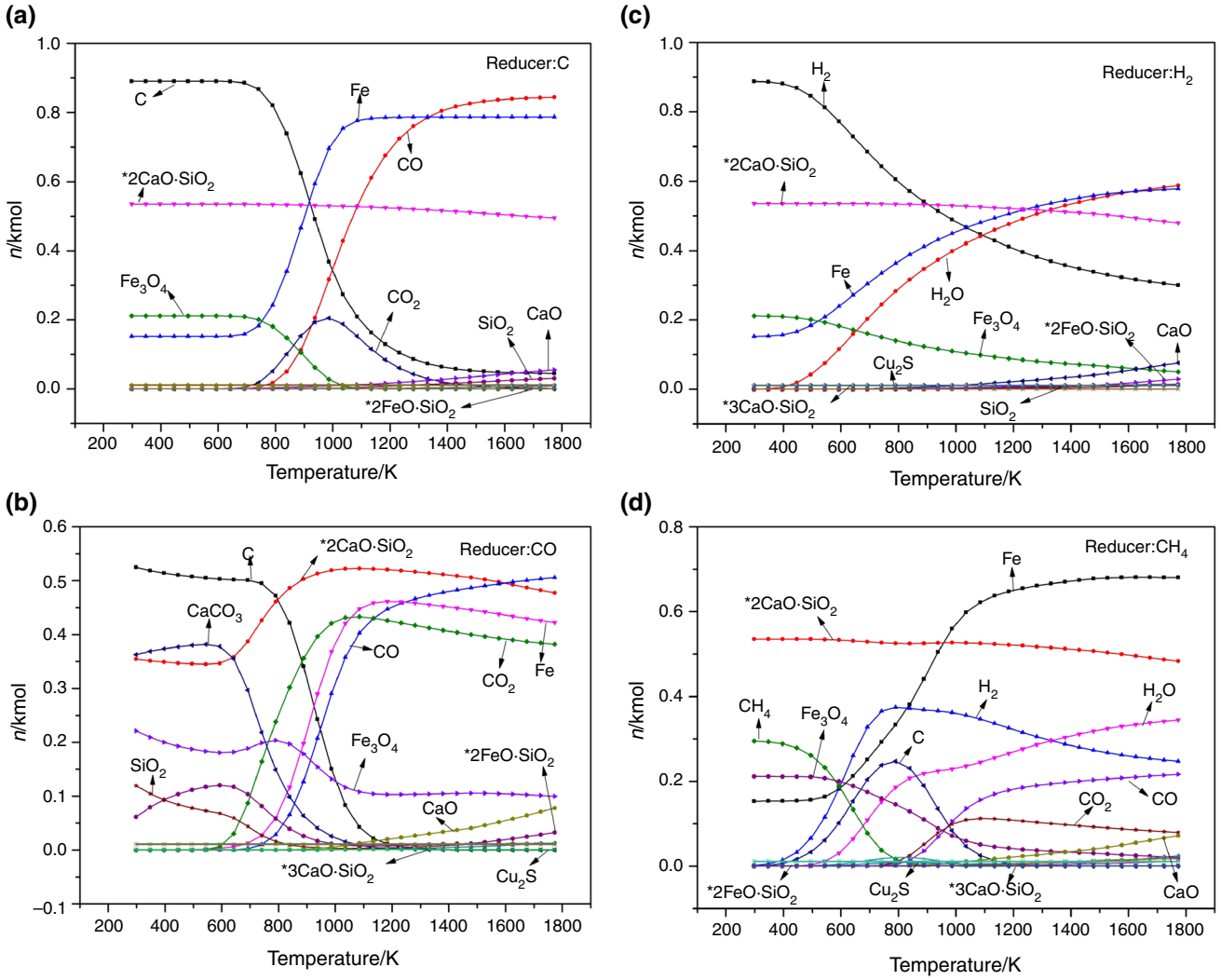

Fig. 4 Effects of temperature on equilibrium compositions

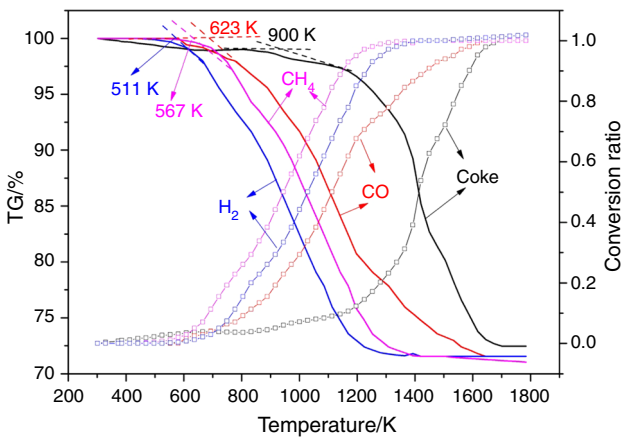

Fig. 5 TG and reduction conversation ratio curves of sample by C, CO, H_2 and CH_4 (Coke is used in experiments on behalf of C)

$$FeO + CO\ (g) = Fe + CO_2\ (g) \quad (5)$$

$$2FeO \cdot SiO_2 + 2CO\ (g) = 2Fe + 2CO_2\ (g) + SiO_2 \quad (6)$$

$$Fe_3O_4 + H_2\ (g) = 3FeO + H_2O \quad (7)$$

$$FeO + H_2\ (g) = Fe + H_2O \quad (8)$$

$$2FeO \cdot SiO_2 + 2H_2\ (g) = 2Fe + 2H_2O + SiO_2 \quad (9)$$

$$3Fe_3O_4 + CH_4\ (g) = 9FeO + 2H_2O + CO_2(g) \quad (10)$$

$$3FeO + CH_4\ (g) = 3Fe + CO_2\ (g) + 2H_2O \quad (11)$$

$$3(2FeO \cdot SiO_2) + 2CH_4\ (g) = 4Fe + 4CO_2\ (g) + 4H_2O + 3SiO_2 \quad (12)$$

$$C + CO_2\ (g) = 2CO\ (g) \quad (13)$$

$$CH_4 + 3CO_2\ (g) = 4CO\ (g) + 2H_2O \quad (14)$$

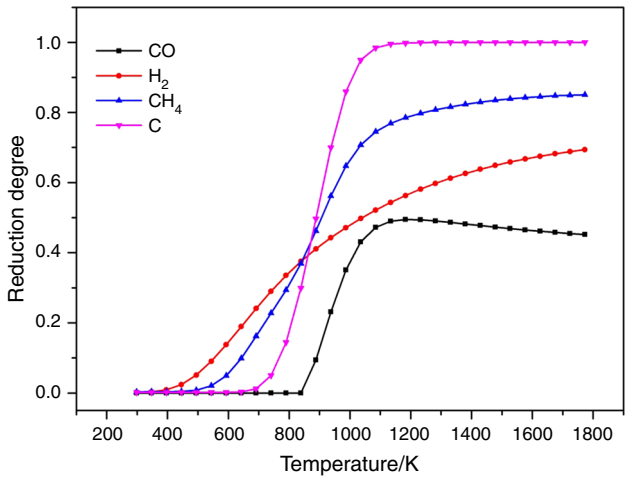

$$2FeO \cdot SiO_2 + 2C + CaO = 2Fe + 2CO\ (g) + CaO \cdot SiO_2 \quad (15)$$

$$2FeO \cdot SiO_2 + 2CO\ (g) + CaO = 2Fe + 2CO_2\ (g) + CaO \cdot SiO_2 \quad (16)$$

$$2FeO \cdot SiO_2 + 2H_2(g) + CaO = 2Fe + 2H_2O + CaO \cdot SiO_2 \quad (17)$$

$$3(2FeO \cdot SiO_2) + 2CH_4\ (g) + 3CaO = 4Fe + 4CO\ (g) + 3CaO \cdot SiO_2 \quad (18)$$

$$CaO + CO_2\ (g) = CaCO_3 \quad (19)$$

$$CH_4\ (g) = C + H_2\ (g) \quad (20)$$

Fig. 6 Effects of temperature on reduction degree

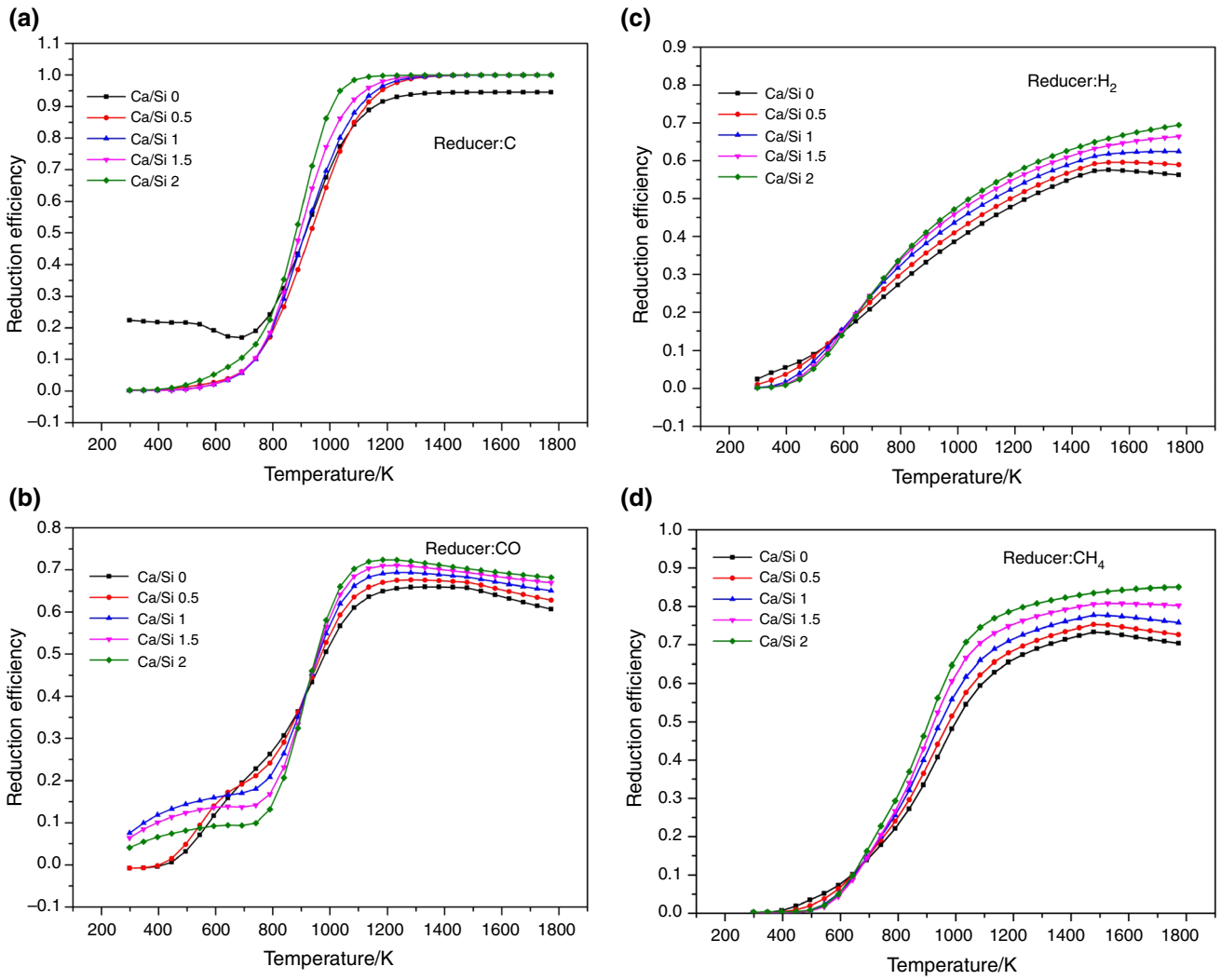

Fig. 7 Effects of CaO addition on reduction degree

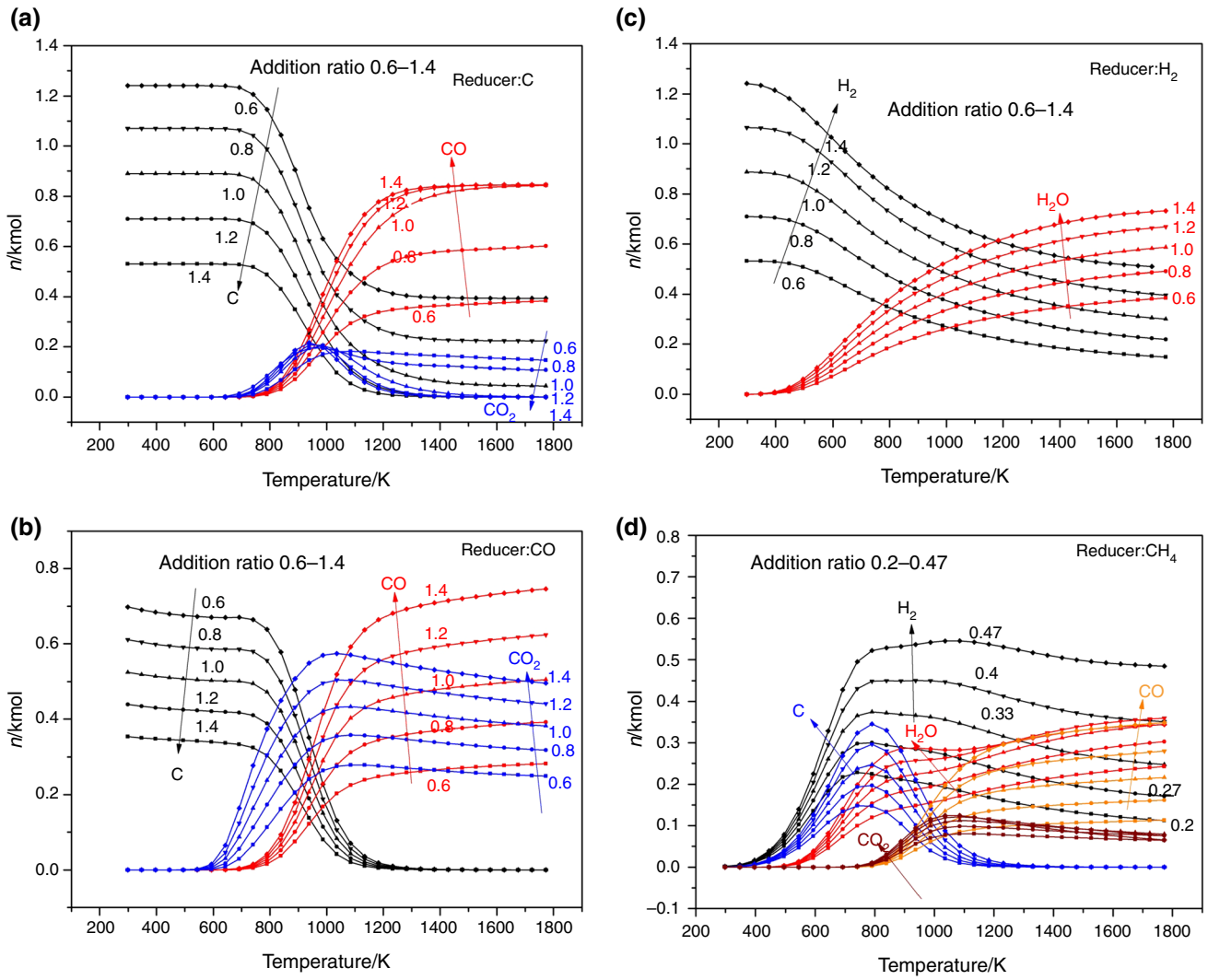

Fig. 8 Effects of reducer addition ratio on gas phase equilibrium composition

Effects of temperature and CaO addition

Effects of temperature on beginning temperature

Equilibrium composition is acquired on the condition that C, CO, H_2 and CH_4 are introduced separately as reducing agent as shown in Fig. 4. Based on Eqs. (1)–(12), theoretical reducer supplementation is selected. The beginning reduction temperatures of H_2, CH_4, C and CO are 396, 445, 593 and 691 K, respectively. The beginning temperature is theoretically confirmed by sudden change data of reduction degree. Thermogravimetric experiments are carried out compared with theoretical calculation results.

A NETZSCH STA409PC thermogravimetric analyzer was employed. Copper slags were mixed thoroughly and then placed in a tungsten crucible. In each experiment, 10 mg of the copper slag was heated from 308 K to 1773 K at a heating rate of 5 K min^{-1}. The protective gas was Ar, and its flow rate was 20 mL min^{-1}, controlled by flow meters. Coke is used to present C. Mixed gas (CO 33% Ar 67%; H_2 33% Ar 67%; CH_4 33% Ar 67%) is inlet, respectively. TG and conversation ratio curves of reduction are shown in Fig. 5. By experiments, the beginning temperature of four kinds of reducer is obtained. Reaction rate affects beginning temperature, different from thermodynamic analysis results above. Affected by diffusion velocity, beginning temperature of solid C is higher than gas reducers. And CH_4 obtains lowest reaction beginning temperature. From Fig. 5, the beginning temperature of C, CO, H_2 and CH_4 is 900, 623, 567 and 511 K, respectively. And the reduction rate of gas reducer is much higher than

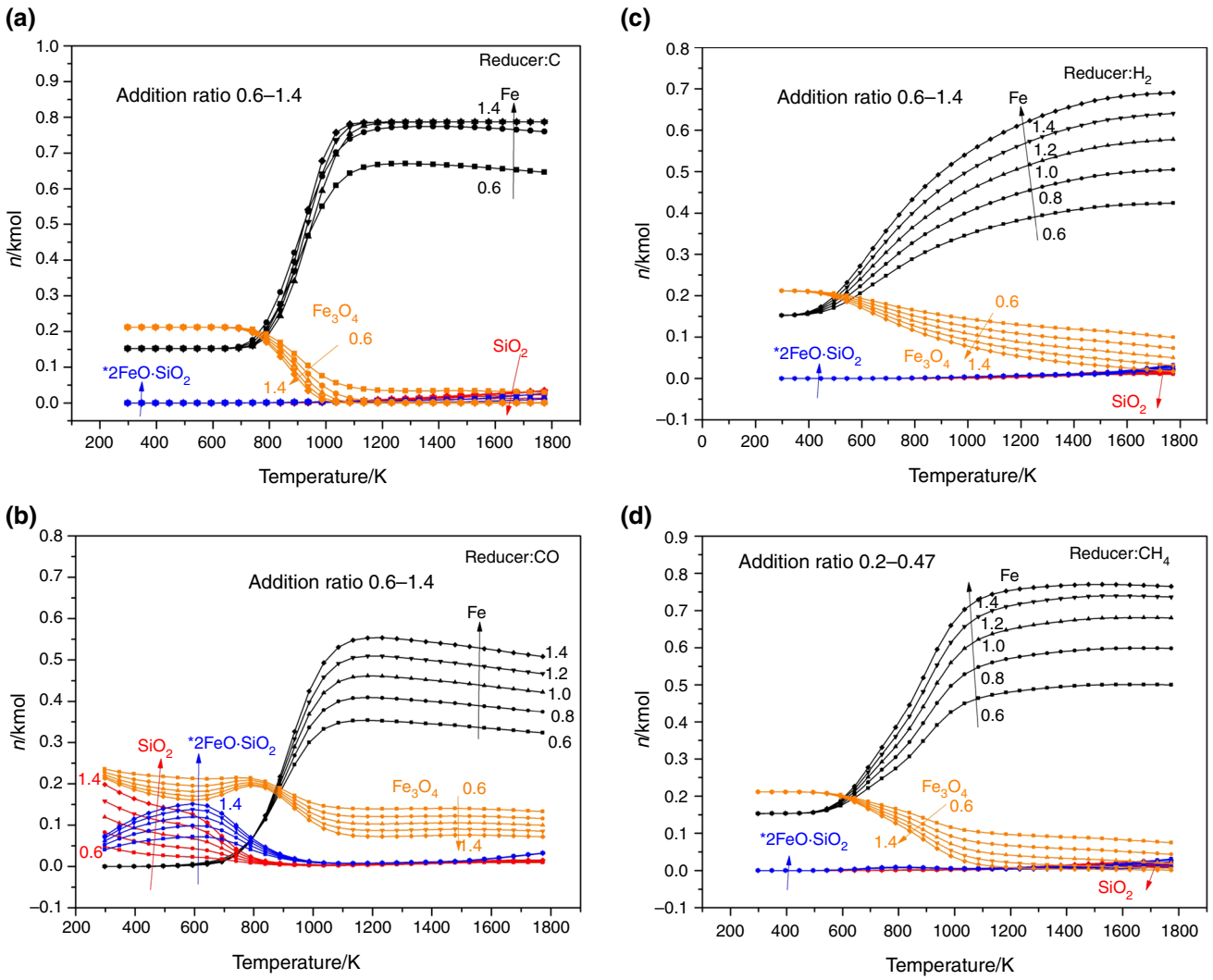

Fig. 9 Effects of reducer addition ratio on Fe, SiO_2 and iron oxide phase equilibrium composition

C. The sequence of reducers by reduction reaction rate is $CH_4 > H_2 > CO$.

Effects of temperature on products

With the increase in temperature, all the reduction reactions are promoted and the molar quantity of Fe increases gradually. As for C, total production of Fe is up to 0.787 kmol when the temperature is at 1379 K. The variation tendency of CO is the same as that of Fe. The variation tendency of C and Fe_3O_4 is the opposite of that of Fe. Due to the promotion function of CaO, the reduction in $2FeO{\cdot}SiO_2$ takes place at room temperature based on the thermodynamic calculation results. The equilibrium compositions of $2FeO{\cdot}SiO_2$ and $2CaO{\cdot}SiO_2$ remain stable. From 700 K to 1400 K, the equilibrium composition of CO_2 increases firstly and then decreases. When the temperature is at 986 K, the equilibrium composition of CO_2 reaches a peak of 0.205 kmol. This is because that when the temperature is lower than 986 K, CO participates in the reduction reactions and CO_2 is generated. When the temperature is higher than 948 and 973 K, the gasification reactions of C with CO_2 take place. And for this reason, the equilibrium composition decreases at high temperature.

The fluctuation tendency of CO and Fe in CO reduction system is similar with that in C reduction system. When the temperature is lower than 600 K, the CO and CO_2 are all transformed into C. When the temperature is higher than 1100 K, the production of Fe decreases slowly. The total production of Fe is 0.5 kmol at 1400 K which is lower than C.

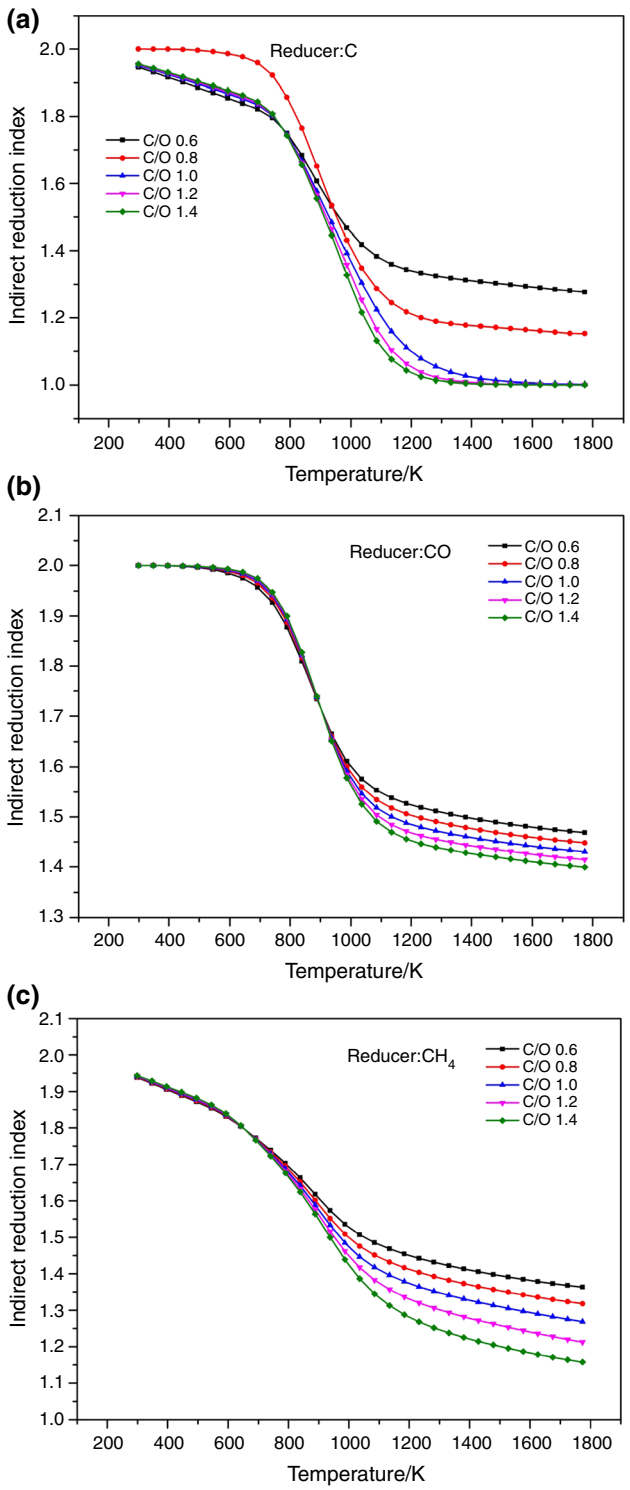

Fig. 10 Effects of reducer addition ratio on indirect reduction index

The reduction in H_2 is accompanied by the production of H_2O. With the increase in temperature, the equilibrium compositions of Fe and H_2O increase gradually. The total production of Fe is 0.578 kmol at 1773 K.

The equilibrium compositions of H_2 and C are increased at the same temperature. This illustrates that decompose reactions of CH_4 take place. With the increase in temperature, H_2O and CO are generated, respectively. And this illustrates that the reduction in H_2 and C takes place at 500 and 800 K, respectively. Compositions of C and H_2 reach a peak at 780 K, and CH_4 decomposes thoroughly at this temperature. And C disappears when the temperature is higher than 1100 K. Residual H_2 exists, and it does not react thoroughly. The total production of Fe reaches to 0.680 kmol at 1773 K.

Effects of temperature on reduction degree

To make sure the reduction degree of the reducers above and the relationships with temperature, reduction degree is determined as follows:

$$\eta = \frac{n_0(\mathrm{FeO}) + 4 \times n_0(\mathrm{Fe_3O_4}) - n_1(\mathrm{FeO}) - 4 \times n_1(\mathrm{Fe_3O_4})}{n_0(\mathrm{FeO}) + 4 \times n_0(\mathrm{Fe_3O_4})} \tag{21}$$

where n_0(FeO) is molar quantity of FeO in copper slag before reduction, $n_0(Fe_3O_4)$ is molar quantity of Fe_3O_4 in copper slag before reduction, n_1(FeO) is molar quantity of FeO in copper slag after reduction and $n_1(Fe_3O_4)$ is molar quantity of Fe_3O_4 in copper slag after reduction.

It is clear from Fig. 6 that the reduction degree of four kinds of reducers is calculated. The reduction degree of C, CH_4, H_2 and CO is 1, 0.851, 0.695 and 0.452, respectively, at 1773 K. In other words, the reduction reaction of C and copper slag is most radical. As shown in Fig. 7, reduction degree is all improved with the addition of CaO for four kinds of reducers.

Effects of reducer addition

Effects of reducer addition on products

To organize reduction reactions of iron oxides, different ratios of reducers are added in this calculation. Based on the current thermodynamic analysis, copper slag is mixed with variable proportions of C, CO, H_2 and CH_4. The C/O, CO/O and H_2/O are in the interval of 0.6–1.2, and the CH_4/O is in the interval of 0.2–0.467. Such conditions and its effects on equilibrium compositions are shown in Figs. 8 and 9. The variation of adding reducers changes the equilibrium compositions. With the increase in reducer addition, compositions of Fe increase and composition of Fe_3O_4 decreases at a different temperature. As shown in Fig. 8a, with the increase in C/O, compositions of C and CO increase on different degrees. Compositions of CO_2 decrease with the increasing addition of reducer, which meant that Eqs. (4)–(6) move backward. As shown in Fig. 8b, with the increase in CO/O, compositions of C, CO

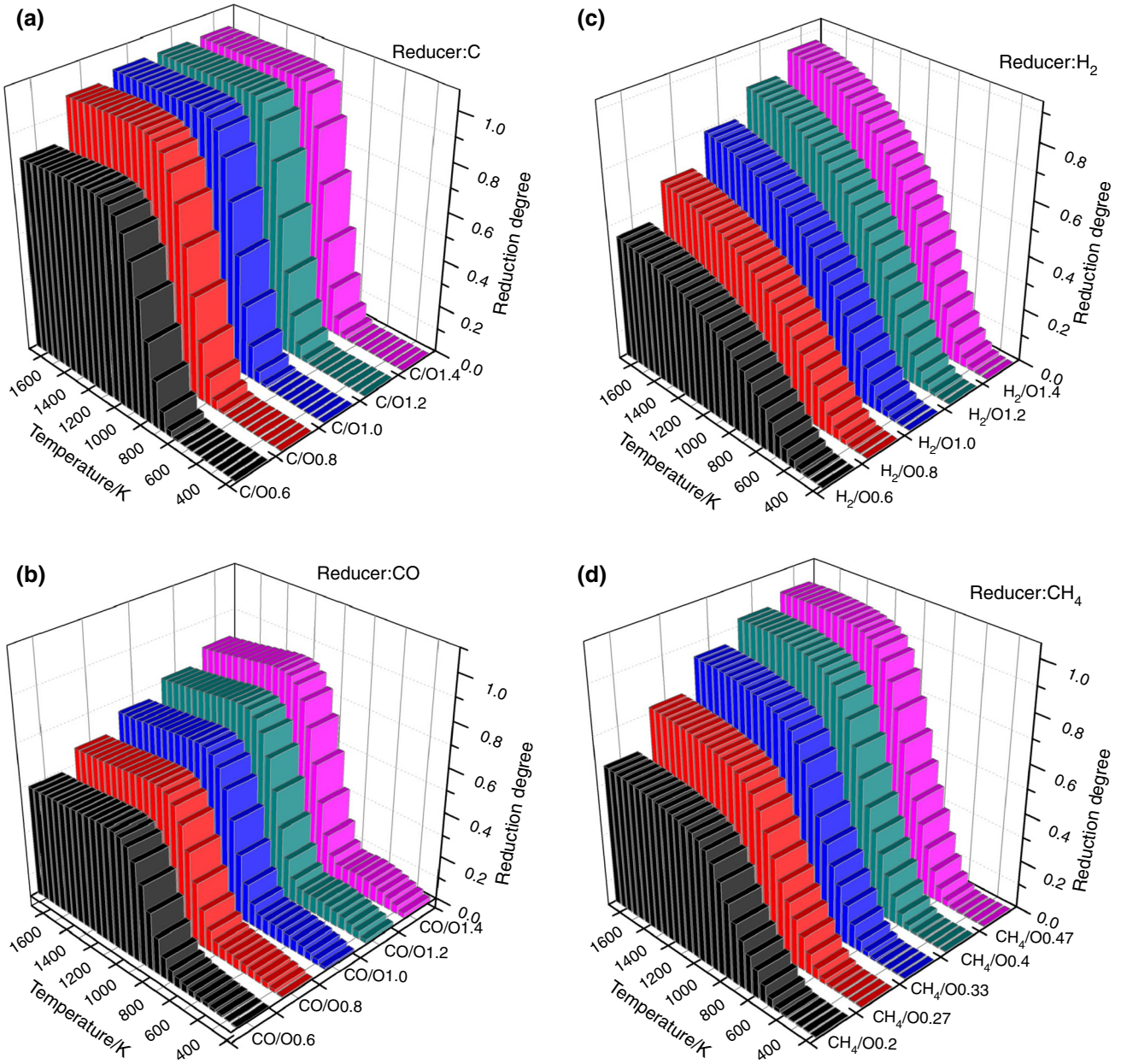

Fig. 11 Effects of reducer addition ratio on reduction degree

and CO_2 increase substantially and CO promotes Eqs. (4)–(6) to move forward. As shown in Fig. 9b, compositions of SiO_2, $2FeO{\cdot}SiO_2$ and Fe_3O_4 fluctuate at low-temperature region. As shown in Figs. 8c and 9c, with the increase in H_2/O, the amplitudes of variation of H_2O and Fe compositions are more obvious. This is because that the high temperature is more beneficial to the reduction in copper slag with H_2 [Eqs. (7)–(9)], which could also be demonstrated in Fig. 6. As shown in Figs. 8d and 9d, with the increase in CH_4/O, compositions of C and H_2O increase at low temperature and composition curves of Fe, Fe_3O_4 and CO_2 transform at high temperature.

Effects of reducer addition on indirect reduction index

The content of C is very important to the reduction in iron oxide in copper slag. The reduction in iron oxide in copper slag contains the reduction in C [Eqs. (1)–(3)] and reduction in CO [Eqs. (4)–(6)], called direct reduction and indirect reduction, respectively. In order to make sure the direct and indirect reduction ratio in every reduction system, indirect reduction index (α) is introduced in this paper. '$\alpha = 1$' represented that there are all direct reductions [Eqs. (1)–(3)]; '$\alpha = 2$' represented that there are all indirect reductions [Eqs. (4)–(6)]; '$1 < \alpha < 2$' represented that

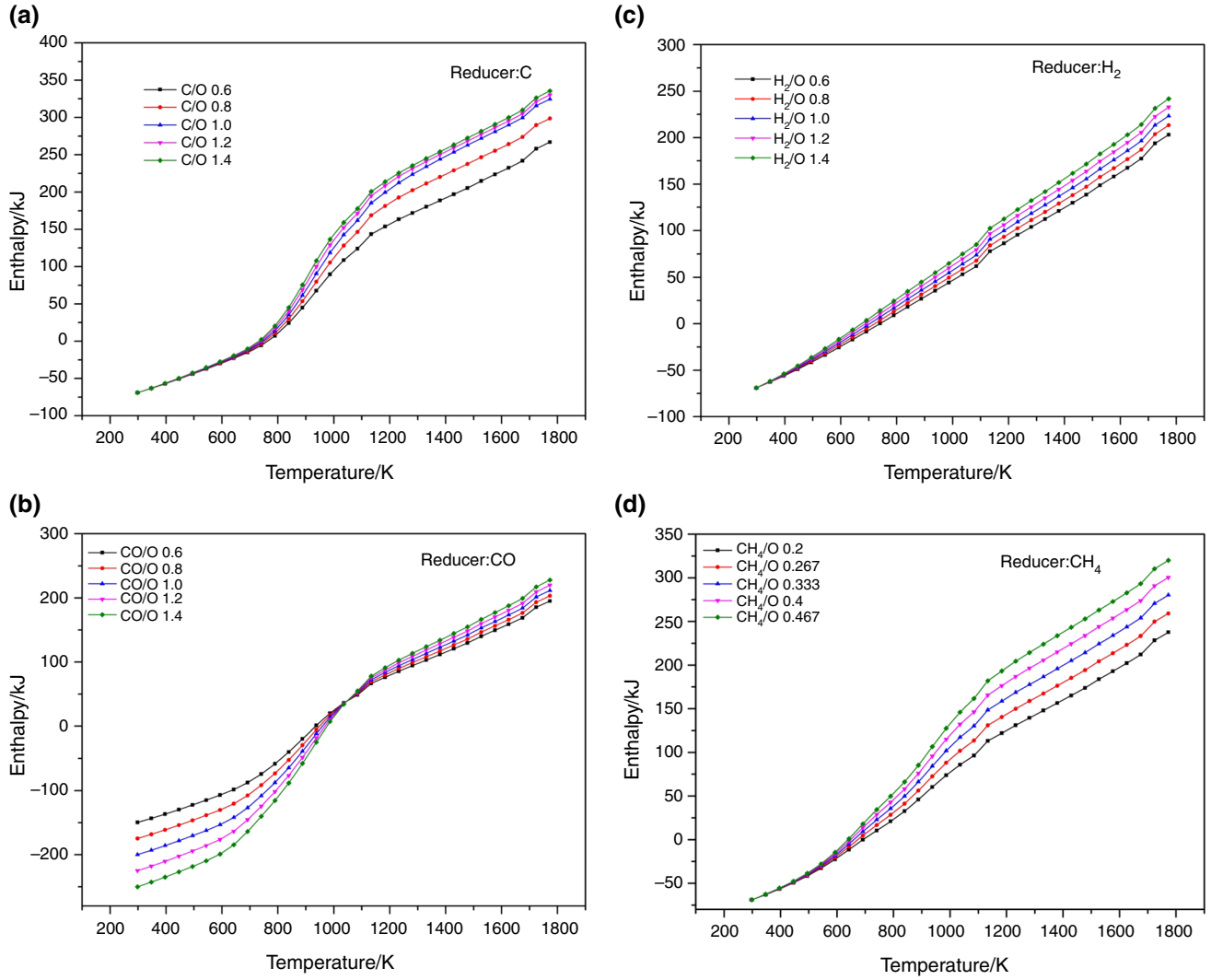

Fig. 12 Effects of reducer addition ratio on enthalpy

there are coexisting status of direct reductions and indirect reductions. α is calculated as follows:

$$\alpha = \frac{n(\mathrm{CO}) + 2 \times n(\mathrm{CO_2})}{n(\mathrm{CO}) + n(\mathrm{CO_2})} \tag{22}$$

where n(CO) is the molar quantity of CO and $n(\mathrm{CO_2})$ is the molar quantity of $\mathrm{CO_2}$.

Reduction reaction index curves are shown in Fig. 10. Indirect reduction index curves are in the shape of reverse 'S.' As shown in Fig. 10a, b, when the temperature is lower than 700 K, indirect reduction reaction index changed slightly and maintains above 1.8 for C and CO reducer. At the temperature region of 700–1173 K which is lower than direct reduction temperature, indirect reduction index decreases dramatically. It means that the direct reduction reactions [Eqs. (1)–(3)] of copper slag dominate at higher temperature and temperature region of 700–1173 K is the transformational zone. For C and CO reducer, indirect reduction index decreases from 1.4 to 1.0 and 1.55 to 1.4, respectively, when the temperature is higher than 1173 K and at the reduction temperature region. As shown in Fig. 10c, when the temperature is lower than 1173 K, indirect reduction reaction index decreased steadily for $\mathrm{CH_4}$ reducer. And at reduction reaction temperature region, indirect reduction index decreases from 1.5 to 1.15.

Effects of reducer addition on reduction degree

Reduction degree curves with the variation of added reducers are shown in Fig. 11. According to Fig. 11a, the value of reduction degree rises from 0.82 to 1 with the increase in C/O when the temperature is above 1173 K. When the reducer addition is above 0.8, reduction degree appears level off. As shown in Fig. 11b, reduction degree rises from 0.52 to 0.77 with the increase in C/O when the temperature is above 1173 K. There is a steady rise of

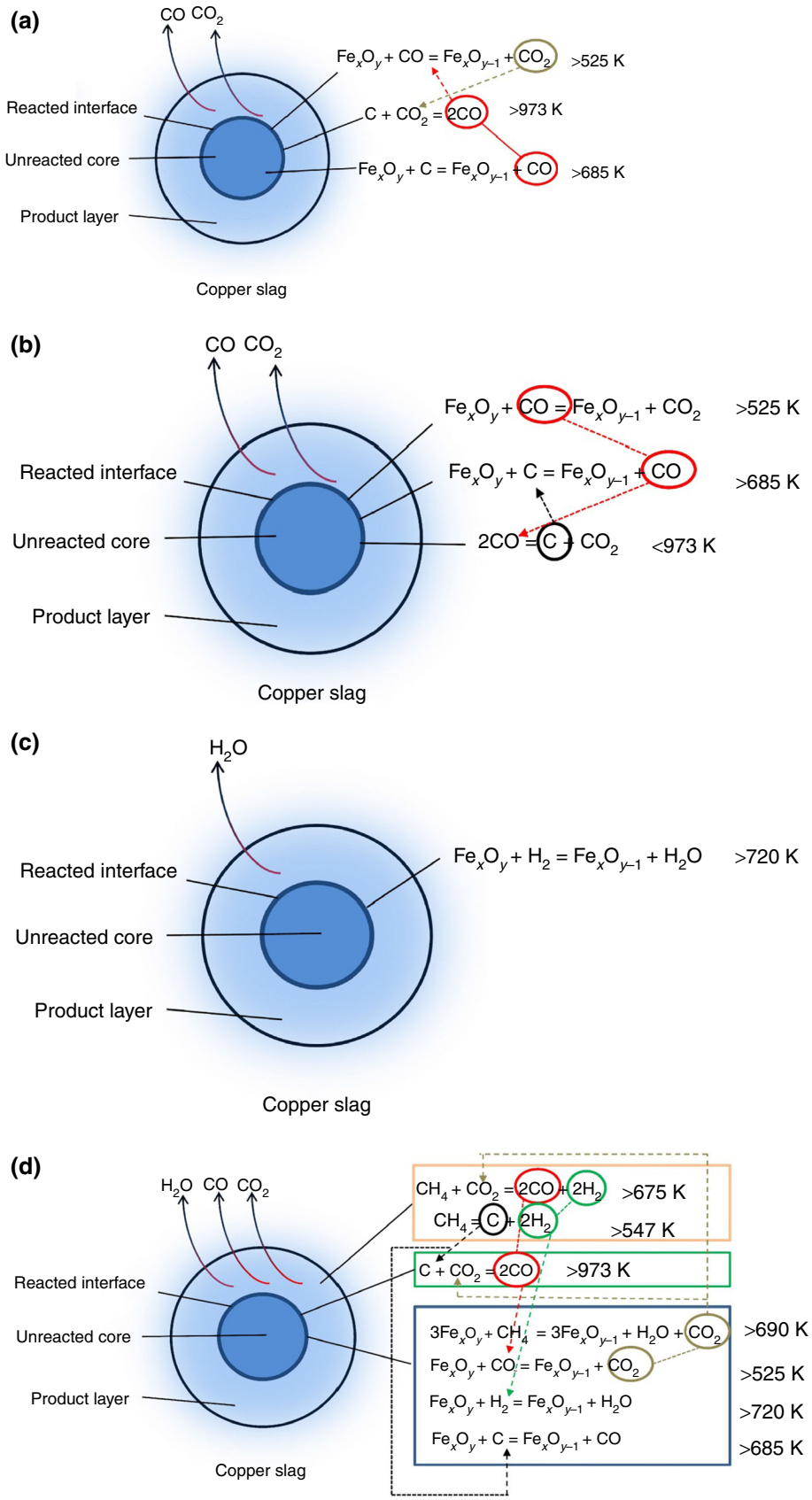

Fig. 13 Reduction reaction path of copper slag by C, CO, H_2 and CH_4: **a** C; **b** CO; **c** H_2; **d** CH_4 (Fe_xO_y represents FeO, Fe_3O_4 and $2FeO{\cdot}SiO_2$)

reduction degree at reduction temperature. Figure 11c, d also describes that the steady rise took place in the value of reduction degree. The figures reach a peak at 0.86 of H_2 reducer and 1 of CH_4 reducer, respectively.

Effects of reducer addition on enthalpy

Enthalpy is basic state parameter of copper slag reduction system. It is significant to study the variation tendency of reduction in copper slag by different kinds of reducers. The reduction in copper slag is endothermic reaction. Based on the calculation of enthalpy, heat supply can be confirmed in theory. As shown in Fig. 12, enthalpy curves varied with the addition of reducers, temperature and reducer types. With the increase in reducer addition, the required quantity of heat increases. The value of enthalpy of four kinds of reducers is in the sequence of $C > CH_4 > H_2 > CO$. For C and CO, there is a growth of enthalpy in the shape of 'S.' Enthalpy increase rate of C and CO at 800–1100 K is higher than the other temperature region. However, for H_2 and CH_4, there is a linear growth of enthalpy with the increase in temperature.

Reduction reaction path of C, CO, H_2 and CH_4

Based on model calculation results and experiment results, reduction reaction path of C, CO, H_2 and CH_4 is simplified. Reduction reaction path of copper slag by C, CO, H_2 and CH_4 is shown in Fig. 13.

Copper slag particle is divided into three reaction regions: unreacted core, reacted interface and product layer. From Fig. 13a, when the temperature is lower than 973 K, C dominates the reduction in copper slag particle. When the temperature is higher than 973 K, gasification reaction of CO_2 consumes C on reacted interface and improves the reduction in CO on reacted interface. From Fig. 13b, CO dominated the reduction in copper slag. However, when the temperature is lower than 973 K, deposition reaction of C takes place and parts of iron oxides are reduced by C to some extent. This phenomenon is also studied by Zhao [35]. As shown in Fig. 13c, the reduction in H_2 takes place on the interface. According to Fig. 13d, the reduction in CH_4 is complicated. C, CO and H_2 participates reduction process as intermediate product. Gasification reaction of CH_4 with CO_2 produces CO and H_2. The crack reaction of CH_4 produces C. The reduction reactions take place on the interface. Similarly, when the temperature is higher than 973 K, gasification of C with CO_2 produces CO and improves reduction reactions.

Conclusions

Thermodynamic study of reduction in copper slag by biomass is conducted based on phase equilibrium calculating model in HSC Chemistry software.

1. The reactions of $2FeO{\cdot}SiO_2$ with C, CO, H_2 and CH_4 could proceed spontaneously with the addition of CaO. The Gibbs free energy decreases significantly by addition of CaO.
2. Beginning temperature of C, CO, H_2 and CH_4 is 900, 623, 567 and 511 K, respectively, based on thermodynamic experiment results. The reduction degree of C, CH_4, H_2 and CO is 1, 0.851, 0.695 and 0.452, respectively, at 1773 K when reducer addition is 1.0. The reduction reaction of C and copper slag is most radical by thermodynamic analysis results. Direct reduction reactions of copper slag dominated at higher temperature, and temperature region of 700–1173 K is the transformational zone.
3. Indirect reduction index curves are in the shape of reverse 'S,' and a higher temperature is in favor of the indirect reduction in copper slag. There is a steady rise in the value of reduction degree with the increase in reducer addition. The value of enthalpy of four kinds of reducers is in the sequence $C > CH_4 > H_2 > CO$.

Acknowledgements The authors would like to acknowledge the support from the Major State Research Development Program of China (2017YFB0603603).

References

1. Alp I, Deveci H, Sungun H. Utilization of flotation wastes of copper slag as raw material in cement production. J Hazard Mater. 2008;159(2–3):390–5.
2. Gorai B, Jana R, K Premchand. Characteristics and utilisation of copper slag—a review. Resour Conserv Recycl. 2003;39(4):299–313.
3. Palacios J, Sánchez M. Wastes as resources: update on recovery of valuable metals from copper slags. Min Proc Ext Met Rev. 2011;120(4):218–23.
4. Yang Z, Lin Q, Xia J, He Y, Liao G, Ke Y. Preparation and crystallization of glass–ceramics derived from iron-rich copper slag. J Alloys Compd. 2013;574:354–60.
5. Liu H, Lu H, Chen D, Wang H, Xu H, Zhang R. Preparation and properties of glass–ceramics derived from blast-furnace slag by a ceramic-sintering process. Ceram Int. 2009;35(8):3181–4.
6. Zhao D, Zhang Z, Tang X, Liu L, Wang X. Preparation of slag wool by integrated waste-heat recovery and resource recycling of molten blast furnace slags: from fundamental to industrial application. Energies. 2014;7(5):3121–35.
7. de Rojas MIS, Rivera J, Frias M, Marin F. Use of recycled copper slag for blended cements. J Chem Technol Biotechnol. 2008;83(3):209–17.
8. Shi C, Meyer C, Behnood A. Utilization of copper slag in cement and concrete. Resour Conserv Recycl. 2008;52(10):1115–20.

9. Heo JH, Kim BS, Park JH. Effect of CaO addition on iron recovery from copper smelting slags by solid carbon. Metall Mater Trans B. 2013;44(6):1352–63.
10. Zhang H, Shi X, Zhang B, Hong X. Reduction of molten copper slags with mixed CO–CH_4–Ar gas. Metall Mater Trans B. 2013;45(2):582–9.
11. Siwiec G, Oleksiak B, Matula T. Reduction of copper slag with the use of carbon granulates. Metalurgija. 2014;53(4):585–7.
12. Zhang J, Qi Y, Yan D. A new technology for copper slag reduction to get molten iron and copper matte. J Iron Steel Res Int. 2015;22(5):396–401.
13. Hu JH, Wang H, Li L. Recovery of iron from copper slag by melting reduction. Kunming: Faculty of Metallurgical and Energy Engineering, Kunming University of Science and Technology; 2011. p. 541–4.
14. Heo JH, Chung Y, Park JH. Recovery of iron and removal of hazardous elements from waste copper slag via a novel aluminothermic smelting reduction (ASR) process. J Clean Prod. 2016;137:777–87.
15. Zhang L, Zhang L, Wang M. Oxidization mechanism in CaO–FeO*x*–SiO_2 slag with high iron content. Trans Nonferr Met Soc. 2006;20(1):79–82.
16. Gyurov S, Rabadjieva D, Kovacheva D, Kostova Y. Kinetics of copper slag oxidation under nonisothermal conditions. J Therm Anal Calorim. 2014;116(2):945–53.
17. Bruckard WJ, Somerville M, Hao F. The recovery of copper, by flotation, from calcium-ferrite-based slags made in continuous pilot plant smelting trials. Miner Eng. 2004;17(4):495–504.
18. Warczok A, Riveros G. Slag cleaning in crossed electric and magnetic fields. Miner Eng. 2007;20(1):34–43.
19. Seo K, Fruehan R. Reduction of FeO in slag with coal char. ISIJ Int. 2000;40(1):7–15.
20. Utigard T, Sanchez G, Manriquez J. Reduction kinetics of liquid iron oxide-containing slags by carbon monoxide. Metall Mater Trans B. 1997;28(5):821–6.
21. Nagasaka T, Hino M, Ban-Ya S. Interfacial kinetics of hydrogen with liquid slag containing iron oxide. Metall Mater Transa B. 2000;31(5):945–55.
22. Strezov V. Iron ore reduction using sawdust: experimental analysis and kinetic modelling. Renew Energy. 2006;31(12):1892–905.
23. Luo S, Yi C, Zhou Y. Direct reduction of mixed biomass-Fe_2O_3 briquettes using biomass-generated syngas. Renew Energy. 2011;36(12):3332–6.
24. de Lima LC. A proposal of an alternative route for the reduction of iron ore in the eastern Amazonia. Int J Hydrogen Energy. 2004;29(6):659–61.
25. Abd Rashid RZ, Mohd SH, Ani MH, Yunus NA, Akiyama T, Purwanto H. Reduction of low grade iron ore pellet using palm kernel shell. Renew Energy. 2014;63:617–23.
26. Guo D, Zhu L, Guo S, Cui B, Luo S, Laghari M, Chen Z, Ma C, Zhou Y, Chen J, Xiao B, Hu M, Luo S. Direct reduction of oxidized iron ore pellets using biomass syngas as the reducer. Fuel Process Technol. 2016;148:276–81.
27. Norgate T, Haque N, Somerville M, Jahanshahi S. Biomass as a source of renewable carbon for iron and steelmaking. ISIJ Int. 2012;52(8):1472–81.
28. Xie H, Yu Q, Zhang Y, Zhang J, Liu J, Qin Q, Zuo Z. New process for hydrogen production from raw coke oven gas via sorption-enhanced steam reforming: thermodynamic analysis. Int J Hydrogen Energy. 2017;42(5):2914–23.
29. Li P. Thermodynamic analysis of waste heat recovery of molten blast furnace slag. Int J Hydrogen Energy. 2017;42(15):9688–95.
30. Zuo Z, Yu Q, Wei M, Xie H, Duan W, Wang K, Qin Q. Thermogravimetric study of the reduction of copper slag by biomass. J Therm Anal Calorim. 2016;126(2):481–91.
31. Li H, Chen Y, Cao Y, Liu G, Li B. Comparative study on the characteristics of ball-milled coal fly ash. J Therm Anal Calorim. 2016;124(2):839–46.
32. Sun Y, Han Y, Wei X, Gao P. Non-isothermal reduction kinetics of oolitic iron ore in ore/coal mixture. J Therm Anal Calorim. 2016;123(1):703–15.
33. Yu W, Tang Q, Chen J, Sun T. Thermodynamic analysis of the carbothermic reduction of a high-phosphorus oolitic iron ore by FactSage. Int J Miner Metall Mater. 2016;23(10):1126–32.
34. Zuo Z, Yu Q, Liu J, Qin Q, Xie H, Yang F, Duan W. Effects of CaO on reduction of copper slag by biomass based on ion and molecule coexistence theory and thermogravimetric experiments. ISIJ Int. 2017;57(2):220–7.
35. Zhao Z, Tang H, Guo Z. Effects of carbon precipitation on reduction of iron oxides under CO atmosphere. J Chin Rare Earth Soc. 2012;30:544–8.